Comprehensive Task Optimization Architecture for Urban UAV-Based Intelligent Transportation System

drones

MDPI

Article

Comprehensive Task Optimization Architecture for Urban UAV-Based Intelligent Transportation System

Marco Rinaldi and Stefano Primatesta *

Department of Mechanical and Aerospace Engineering, Politecnico di Torino, Corso Duca degli Abruzzi 24, 10129 Torino, Italy; marco_rinaldi@polito.it
* Correspondence: stefano.primatesta@polito.it

Abstract: This paper tackles the problem of resource sharing and dynamic task assignment in a task scheduling architecture designed to enable a persistent, safe, and energy-efficient Intelligent Transportation System (ITS) based on multi-rotor Unmanned Aerial Vehicles (UAVs). The addressed task allocation problem consists of heterogenous pick-up and delivery tasks with time deadline constraints to be allocated to a heterogenous fleet of UAVs in an urban operational area. The proposed architecture is distributed among the UAVs and inspired by market-based allocation algorithms. By exploiting a multi-auctioneer behavior for allocating both delivery tasks and re-charge tasks, the fleet of UAVs is able to (i) self-balance the utilization of each drone, (ii) assign dynamic tasks with high priority within each round of the allocation process, (iii) minimize the estimated energy consumption related to the completion of the task set, and (iv) minimize the impact of re-charge tasks on the delivery process. A risk-aware path planner sampling a 2D risk map of the operational area is included in the allocation architecture to demonstrate the feasibility of deployment in urban environments. Thanks to the message exchange redundancy, the proposed multi-auctioneer architecture features improved robustness with respect to lossy communication scenarios. Simulation results based on Monte Carlo campaigns corroborate the validity of the approach.

Keywords: auction; multi-robot task allocation; intelligent transportation system; UAV; drone delivery; aerial robotics; task scheduling; path planning; aerial package delivery; UAS; dynamic task

Citation: Rinaldi, M.; Primatesta, S. Comprehensive Task Optimization Architecture for Urban UAV-Based Intelligent Transportation System. *Drones* **2024**, *8*, 473. https://doi.org/10.3390/drones8090473

Academic Editor: Peiying Zhang

Received: 26 July 2024
Revised: 3 September 2024
Accepted: 8 September 2024
Published: 10 September 2024

Correction Statement: This article has been republished with a minor change. The change does not affect the scientific content of the article and further details are available within the backmatter of the website version of this article.

1. Introduction

The versatility of Unmanned Aerial Vehicles (UAVs), i.e., drones, is such that they are being extensively integrated into the technology of Intelligent Transportation Systems (ITSs) nowadays [1]. Both the efficiency and the sustainability of the ITS technology can be enhanced by the integration of drones, making UAVs a revolutionizing technology in this sector. The applications of UAVs in the ITS context are being developed by researchers and companies all over the world, with a particular focus on urban applications [2]. The main applications include, but are not limited to, traffic and environmental monitoring, infrastructure inspection, aerial mapping, surveillance, emergency management, data collection, and logistics [3].

Considering the drone delivery application in an urban environment, which is the main focus of this work, UAVs are seen as a strategic technological advancement for addressing the challenges of urban transportation, being able to reduce the environmental impact of the transportation network as well as reduce costs and delivery time [4]. Whether UAVs operate in cooperation with traditional transportation systems, e.g., trucks, or they constitute a transportation system on their own, their capability of enhancing the sustainability and efficiency of the delivery process is unquestionable. This is mainly due to the capability of drones to (i) navigate the crowded urban environment with ease, independently of both the complexity of the urban landscape and the road traffic conditions; (ii) reduce both urban traffic congestion and delivery costs, especially in case of small-package delivery, with

superior efficiency with respect to trucks; (iii) enable delivery services in areas difficult of reach by conventional ground vehicles or areas hit by natural disasters; (iv) enable on-demand dynamic delivery services with reduced waiting times for customers; (v) collect real-time data to be included into smart city platforms, thus enabling the continuous optimization of the delivery service itself as well as improving decision-making capabilities in a smart city context; (vi) rapidly perform medical deliveries, and (vii) offer a variety of simultaneous services throughout their operation for transportation purposes, such as data analysis, prediction of patterns, etc. [5,6].

On the other hand, the drone technology still faces some technical, environmental, regulatory, and societal barriers for its large-scale deployment in urban environments [7]. Limited flight range due to battery capacity, energy consumption, integration into the current airspace, licensing of pilots, noise pollution, safety and security risks, poor withstanding capability of adverse weather conditions, privacy concerns, infrastructure requirements, and high initial costs are some of the main challenges that have not been completely addressed yet [8]. Therefore, the sustainability of UAV-based ITSs will require a non-trivial joint effort from regulators, researchers, logistics and drone companies, and urban planners to overcome the current barriers that limit the real-world applicability of unmanned aerial networks in smart cities.

When dealing with a multi-robot system, such as an ITS based-on UAVs [9–12], the conceptualization of a task allocation architecture is needed to enable an optimal distribution of tasks among the robots. The Multi-Robot Task Allocation (MRTA) problem is a variant of the well-known NP-hard Traveling Salesman Problem (TSP), and several suboptimal approaches have been proposed in the literature [13–16]. The main task allocation algorithms for UAV networks proposed in the literature are deterministic algorithms [17], stochastic algorithms [18], auction-based algorithms [19], bio-inspired algorithms [20], and edge-computing algorithms [21]. Depending on the communication architecture implemented in the multi-agent system, MRTA algorithms can be classified as centralized, decentralized, and distributed. The latter refers to a case where the architecture is hybrid. In centralized task allocation architectures, a central coordinator (considering the information shared by the other robots) allocates the tasks to the robots, maximizing the global utility of the multi-robot system. On the other hand, in a decentralized architecture, the tasks are allocated to the robots according to the partial knowledge of the environment that each robot has. Market-based allocation strategies are widely used to assign tasks (items) in multi-robot systems since they represent an effective and intuitive way of accounting for different robots' costs with respect to the tasks to be allocated [22]. Auction-based algorithms feature, in general, polynomial computational complexity and are suitable for every type of communication architecture. A classical auction-based task allocation algorithm works according to a communication protocol between a central allocating robot (auctioneer) and the other robots of the system (bidders). The protocol is repeated for every round of allocation. The total number of rounds depends on the number of tasks advertised and allocated per round, and the auction algorithm is defined as either multiple-item or single-item accordingly. A standard auction-based allocation protocol consists of four Phases (P), as follows:

- Advertisement (P_1): the auctioneer broadcasts the task to the robots of the network.
- Bidding (P_2): each robot undergoes a task valuation process and sends its bid to the auctioneer.
- Award (P_3): the auctioneer selects the most suitable robot for the task based on all the received bids for that task.
- Acknowledgment (P_4): each robot acknowledges the assignment to the auctioneer.

A schematic representation of the process is presented in Figure 1.

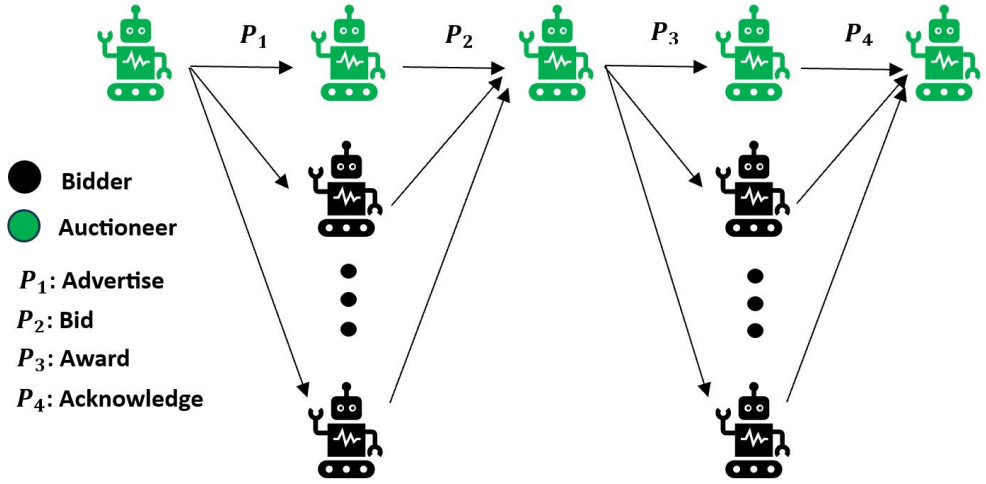

Figure 1. Schematic representation of the standard four phases of an auction-based allocation round in a centralized multi-robot system.

One of the main advantages of auction-based optimization is the low computational complexity and the ease of hybridization with other optimization approaches. The work in [23] proposed a dynamic task allocation framework based on the decomposition of the task assignment problem into two sub-problems, i.e., group-level task assignment and member-level task assignment. The sub-problems were then solved by using Particle Swarm Optimization (PSO) together with distributed auctions. A distributed sequential auction allocation strategy was proposed in [24] to tackle the multi-UAV target task allocation problem with limited communication range. Detected targets are advertised sequentially and, depending on the decision of neighbor UAVs, each UAV decides whether to auction or forfeit the target. A simulation study conducted with different communication ranges proved the superiority of the distributed sequential auction strategy with respect to a simpler greedy allocation. Auction algorithms are also exploited for assigning tasks in dynamic and changeable environments, such as the battlefield environment. The problem of optimal task rescheduling in such a scenario was addressed in [25], and a distributed task scheduling algorithm was proposed. By means of a result update strategy, the original schedule of tasks undergoes a partial reset, and re-planning aiming at payoff maximization is performed by means of the proposed online auction mechanism. Auction algorithms are also popular because they can abstract the characteristics and the limitations of the multi-robot system with respect to the tasks. As shown in [26], a distributed auction-based assignment strategy for search and destroy missions carried out by Miniature Aerial Vehicles (MAVs) was implemented and tested for different target distributions and sensor ranges. Combinatorial auction-based strategies [27,28] also represent an efficient and scalable sub-optimal solution to the TSP and its variants, such as last-mile delivery with drones and, in general, Multi-Unmanned Aerial Vehicle Task Allocation (MUAVTA). Applications for the optimal scheduling of air taxi operations in an urban air mobility context can be found in [29].

This paper is a follow-up to a previous work on a centralized market-based task allocation architecture for a drone-based parcel pick-up and delivery system [30]. Such work consisted of (i) the formalization of a persistent drone delivery problem that takes into account the safety of UAV flyable paths, UAV battery discharge, task due dates, and UAV energy consumption for task execution, (ii) the design and implementation of a dynamic-auctioneer auction-based task scheduling architecture distributed among the UAVs of the network, (iii) the integration of a risk-aware path planning strategy with an energy consumption-aware velocity optimizer of task execution within the task scheduling framework, and (iv) the evaluation of the proposed approach with a real-world aerial delivery scenario in the city of Turin, Italy. Moreover, the impact of fallible communication among the drones on the overall assignment of tasks was simulated, highlighting an

increasing number of unassigned tasks in the final solution for increasing probability of communication losses in the network.

In this work, the market-based task assignment architecture proposed in [30] is extended to enable both resource sharing for an even distribution of tasks in the fleet and allocation of dynamic tasks during each round of the main allocation process. Starting from the same task allocation architecture proposed in [30], a hybrid variable-auctioneer auction-based allocation of tasks is nested into the main sequential single-item algorithm. In this way, besides the allocation of "regular" delivery tasks and re-charge tasks, tasks with higher priority can be allocated dynamically to the UAVs while the main multi-auctioneer algorithm is being executed. Moreover, the message exchange in the novel distributed architecture is more redundant than the one in the previous work. As such, an increased robustness of the aerial network with respect to communication failures is obtained. The literature gaps covered in this work are highlighted in the following:

- Formalization of an original drone delivery problem (DDP) with charging hubs, including risk-aware route planning, dynamic task allocation, and balance of number of assigned tasks to each UAV.
- Development of a comprehensive allocation framework for tackling the formulated problem, optimizing energy efficiency, risk of flyable paths, and flight time.
- Inclusion of a redundant allocation strategy within the formulated architecture to address lossy communication scenarios.

We advance the state-of-the-art about auction-based task allocation for UAV networks by not only proposing a combined auction-based task scheduling and path planning heuristic solution to a drone pick-up and delivery problem with charging hubs, but also considering dynamic assignment of tasks with high priority within the allocation protocol and the problem of resource sharing in the multi-robot system.

This paper is organized as follows. In Section 2, the addressed problem is defined, as well as the assumptions. Section 3 presents the comprehensive auction-based allocation architecture, including the allocation algorithm, the energy consumption model, the optimization algorithm, and the path planning approach. Simulation results are reported in Section 4. Conclusions are drawn in Section 5.

2. Problem Statement

The problem addressed in this work can be defined as a combined task allocation and path planning problem to enable a persistent UAV-based intelligent transportation system in urban environments. It follows the formalization of the aerial delivery scenario:

- The multi-robot system consists of multi-rotor UAVs operating in a well-defined populated urban operational area with charging stations.
- The task set consists of payload transportation tasks within the operational area. Each task is defined as the transportation of a payload mass from a pick-up location to a delivery location within a delivery time window.

The formulated problem is to define an optimization-based combined task scheduling and path planning architecture in order to allocate the delivery tasks to the fleet of UAVs, with the following objectives:

- Minimize the total energy consumption required by the UAVs to execute all tasks.
- Minimize the discrepancy in the number of allocated tasks to each drone, i.e., maximize the workload homogeneity in the fleet of UAVs.
- Enable the allocation of dynamic tasks with higher priority with respect to the "regular" set of transportation tasks. An example is represented by the unexpected aerial delivery of medical samples to a hospital located in the operational area.
- Maximize the safety of the community and the feasibility of deployment of the aerial system in the real world by predicting risk-aware flyable paths to be executed by the UAVs [31].

To improve the clarity of the problem statement, the notations used in this section are provided in a dedicated "Nomenclature" section at the end of the manuscript, which includes a complete list of symbols adopted in this work.

Figure 2 represents a simplified example of the problem with three drones, three delivery tasks, and one charge hub in the city of Turin, Italy.

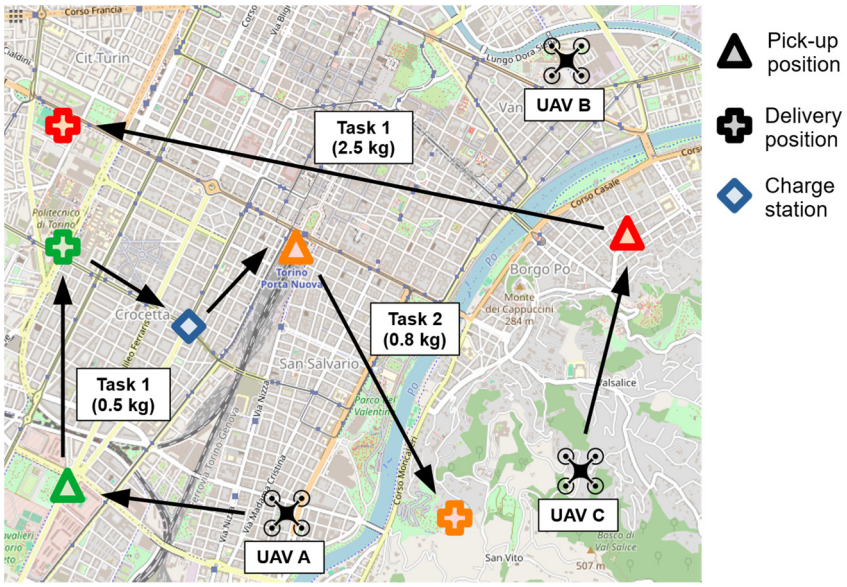

Figure 2. Schematic representation of the addressed drone delivery problem with three UAVs, three tasks, and one charge hub in the urban operational area defined in the city of Turin, Italy.

To address the problem formulated above, the following simplifying assumptions were made:

- The payload capacity of a UAV equals its mass.
- A UAV can carry one payload at a time.
- A UAV cannot visit a charge station in loaded conditions.
- At the beginning of the delivery process, the UAVs are fully charged.
- The UAV re-charge time is the sum of the battery re-charge time (linearly interpolated from the residual battery level of the UAV) and the time needed by the UAV to reach the charge hub.
- A delivery task consists of six consecutive phases: unloaded UAV take-off, unloaded UAV cruise, unloaded UAV landing (the parcel pick-up phase takes place in unloaded conditions), loaded UAV take-off, loaded UAV cruise, and loaded UAV landing (the parcel delivery phase takes place in loaded conditions).
- A re-charge task consists of three consecutive phases: UAV take-off, UAV cruise, and UAV landing. In this case, no payload is carried by the UAV.
- UAVs maintain constant velocity throughout each phase of task execution, i.e., UAVs ascend at constant speed, cruise at constant speed, etc.
- UAV tilt angles are small throughout the flight.
- Turbulent atmospheric phenomena are neglected.

A residual battery level was imposed to each UAV in order to cover the worst-case scenario, i.e., both the UAV and the charge hub were located at the extremities of the operational area. E_{MIN} is predicted by the following optimization problem:

$$E_{MIN} = \min E_{CT}(\boldsymbol{V_{CT}}), \text{subject to :} \tag{1}$$

$$h\left(\frac{1}{V_1'} - \frac{1}{V_3'}\right) + \frac{d_{MAX}}{V_2'} \leq \Delta T_{MAX} \tag{2}$$

$$E_{CT}(\boldsymbol{V_{CT}}) \leq E_{MAX} \tag{3}$$

$$\boldsymbol{V_{LB}} < \boldsymbol{V_{CT}} < \boldsymbol{V_{UB}} \tag{4}$$

with $\boldsymbol{V_{UB}} = [V_{MAX},\ V_{MAX}, 0]$ and $\boldsymbol{V_{LB}} = [0,\ 0, -V_{MAX}]$. $\boldsymbol{V_{CT}} = \left[V_1', V_2', V_3'\right]$ denotes the UAV velocity vector for a re-charge task. Equation (1) minimizes the UAV energy to reach a charge station while considering the constraints on (i) maximum allowable flight time to the charge station itself in the worst-case scenario (Equation (2)), (ii) maximum energy stored in the UAV battery (Equation (3)), and (iii) maximum and minimum UAV velocities during the three phases of a re-charge task (take-off, cruise, and landing), as per Equation (4).

The UAV optimal velocity of execution of a "regular" delivery task is predicted as follows:

$$\boldsymbol{V_{DT}^*} = \arg[\min E_{DT}(\boldsymbol{V_{DT}})], \text{subject to :} \tag{5}$$

$$T_i + h\left(\frac{1}{V_1} - \frac{1}{V_3} + \frac{1}{V_4} - \frac{1}{V_6}\right) + \frac{L_1}{V_2} + \frac{L_2}{V_5} \geq T_{MIN} \tag{6}$$

$$T_i + h\left(\frac{1}{V_1} - \frac{1}{V_3} + \frac{1}{V_4} - \frac{1}{V_6}\right) + \frac{L_1}{V_2} + \frac{L_2}{V_5} \leq T_{MAX} \tag{7}$$

$$E_{DT}(\boldsymbol{V_{DT}}) \leq E_U - E_{MIN} \tag{8}$$

$$\boldsymbol{V_{LB}} < \boldsymbol{V_{DT}} < \boldsymbol{V_{UB}} \tag{9}$$

with $\boldsymbol{V_{UB}} = [V_{MAX}, V_{MAX}, 0, V_{MAX}, V_{MAX}, 0]$ and $\boldsymbol{V_{LB}} = [0, 0, -V_{MAX}, 0, 0, -V_{MAX}]$. The energy consumption predicted for the completion of a delivery task is $E_{DT}^* = E_{DT}(\boldsymbol{V_{DT}^*})$. $\boldsymbol{V_{DT}} = [V_1, V_2, V_3, V_4, V_5, V_6]$ denotes the UAV velocity vector for a delivery task. In Equation (5), the UAV optimal velocity of execution of a delivery task is computed by minimizing the energy required to execute that task, subject to the constraints that (i) the task is delivered within the due date window, as per Equations (5) and (6), (ii) the UAV does not run out of energy, as per Equation (8), and (iii) maximum and minimum UAV velocities for the six phases of a delivery task are respected.

The optimal velocity of execution of a re-charge task is predicted as follows:

$$\boldsymbol{V_{CT}^*} = \arg\left[\min\left(h\left(\frac{1}{V_1'} - \frac{1}{V_3'}\right) + \frac{d}{V_2'}\right)\right], \text{subject to :} \tag{10}$$

$$E_U - E_{CT}(\ \boldsymbol{V_{CT}}) \geq 0 \tag{11}$$

$$\boldsymbol{V_{LB}} < \boldsymbol{V_{CT}} < \boldsymbol{V_{UB}} \tag{12}$$

Equation (10) computes the optimal velocity of execution of a re-charge task by minimizing the flight time to the charge station, subject to the constraints that (i) the UAV does not run out of battery before reaching the charge hub, as per Equation (11), and (ii) maximum and minimum UAV velocities for the three phases of a re-charge task are respected.

The UAV optimal velocity of execution of a dynamic delivery task with high priority is predicted as follows:

$$\boldsymbol{V_{DDT}^*} = \arg\left[\min h\left(\frac{1}{V_1''} - \frac{1}{V_3''} + \frac{1}{V_4''} - \frac{1}{V_6''}\right) + \frac{L_1}{V_2''} + \frac{L_2}{V_5''}\right], \text{subject to :} \tag{13}$$

$$T_i + h\left(\frac{1}{V_1''} - \frac{1}{V_3''} + \frac{1}{V_4''} - \frac{1}{V_6''}\right) + \frac{L_1}{V_2''} + \frac{L_2}{V_5''} \geq T_{MIN} \tag{14}$$

$$T_i + h\left(\frac{1}{V_1''} - \frac{1}{V_3''} + \frac{1}{V_4''} - \frac{1}{V_6''}\right) + \frac{L_1}{V_2''} + \frac{L_2}{V_5''} \leq T_{MAX} \tag{15}$$

$$E_{DDT}(\boldsymbol{V_{DDT}}) \leq E_U \tag{16}$$

$$\boldsymbol{V_{LB}} < \boldsymbol{V_{DDT}} < \boldsymbol{V_{UB}} \quad (17)$$

The optimal energy consumption related to the completion of a dynamic delivery task is $E^*_{DDT} = E_{DDT}\left(\boldsymbol{V^*_{DDT}}\right)$. $\boldsymbol{V_{DDT}} = \left[V''_1, V''_2, V''_3, V''_4, V''_5, V''_6\right]$ denotes the UAV velocity vector for a dynamic delivery task. Equation (13) computes the optimal UAV velocity for a dynamic delivery task, minimizing the flight time, subject to the constraints that (i) the task is delivered within the due date window, as per Equations (14) and (15), (ii) the UAV does not run out of energy before completing the task, as per Equation (16), and (iii) maximum and minimum UAV velocities for the six phases of a delivery task are respected. It is worth noticing that after the completion of a dynamic task, the UAV may have no residual energy in the battery. This is due to the priority of the dynamic task, which overrides the constraint on E_{MIN} introduced for formulating a persistent drone delivery system. For the sake of clarity, it is hereby specified that landing velocities are considered as negative.

3. Task Allocation Architecture

The proposed market-based task optimization architecture is conceptualized as a distributed combined task allocation and path planning architecture. The market-based architecture consists of a central allocator (the coordinator of the fleet of UAVs) with auctioneer behavior that allocates the delivery tasks to the UAVs of the fleet. Each UAV runs, in a decentralized way, both a risk-aware path planner and an optimization algorithm to (i) compute both the optimal path for the task and the optimal velocity of execution for the task, and (ii) bid for the advertised task. The architecture is implemented in MATLAB/ROS. The communication between the UAVs throughout the allocation process is simulated by means of ROS nodes and a publisher/subscriber logic. Besides the main allocation process of the delivery task set, each UAV features an auctioneer behavior when the allocation of a re-charge task is needed to preserve the persistency of the aerial UAV-based ITS. A sequential single-item auction-based allocation strategy is implemented for the allocation of the delivery tasks, while a multiple-item auction-based strategy is implemented for the allocation of the re-charge tasks. This is because sequential single-item allocation strategies represent a better strategy for tasks with different priorities and different due dates (as for the commercial parcel delivery use case of this work). On the other hand, since multiple re-charge tasks (corresponding to the multiple charge hubs in the operational aera) have to be evaluated by the UAV to be charged before the allocation is performed, a multiple-item allocation strategy is preferred for this type of task. The fleet coordinator retains the delivery task set, while dynamic tasks, such as the delivery of medical samples with high priority, can be broadcasted to all the UAVs of the aerial ITS at any time. During the bidding phase for a "regular" delivery task, another single-item allocation is enabled such that the bidding UAV temporarily becomes the auctioneer of the network in order to (i) be able to allocate, if present, a dynamic task with high priority within the main allocation process, and (ii) bid for the "regular" delivery task advertised by the fleet coordinator in that round while being aware of the current workload distribution in the fleet. The communication among the UAVs of the network is assumed to be potentially fallible, apart from the messages from auctioneer to auctioneer, which are never lost.

A schematic representation of the distributed multi-auctioneer behavior of the UAV network is provided in Figure 3. In particular, Figure 3 represents a snapshot of a possible set of roles of the UAVs of the network within a task allocation round, with UAV N being the fleet coordinator (auctioneer of delivery tasks), UAV i $(i = 1, \ldots, N-1)$ being the coordinated robot (bidder for delivery tasks), each UAV beside the fleet coordinator being the auctioneer of a re-charge task, and UAV 1 being the auctioneer of a dynamic high-priority task arising during its bidding phase for a "regular" delivery task.

The allocation algorithm is presented in detail in Section 3.1, while the path planning algorithm, the energy consumption model, and the optimizer are presented in Section 3.2, Section 3.3, and Section 3.4, respectively.

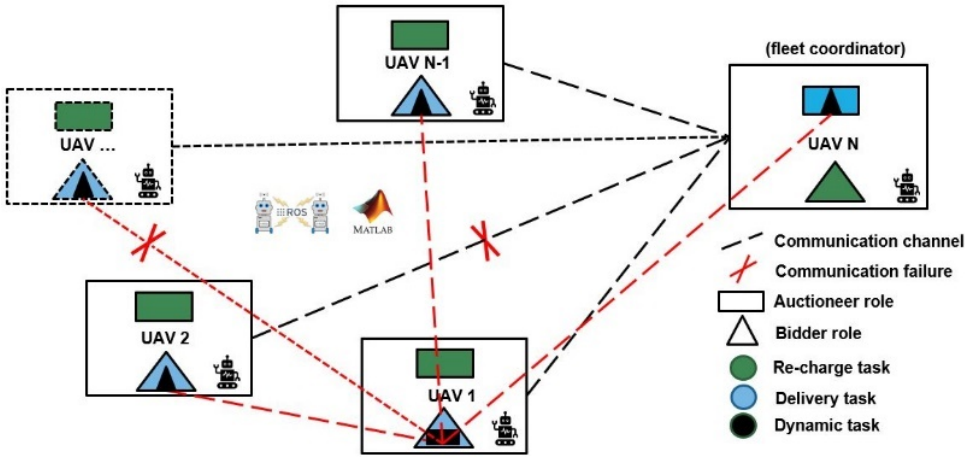

Figure 3. Conceptualization of the architecture with nested dynamic task allocation: example of the dynamic role of each UAV in the auction-based allocation architecture (shown for the bidding phase of UAV 1), where each UAV can serve as both an auctioneer and a bidder throughout the task allocation process.

3.1. Market-Based Task Scheduling

The proposed market-based task optimization algorithm is reported in Algorithm 1.

The computational complexity of Algorithm 1, which also includes Algorithms 2 and 3, is polynomial and is defined as $O(MNB + MN^2)$. Therefore, the approach is highly scalable with respect to the number of drones, tasks, and re-charge hubs.

Algorithm 2 presents the auction-based algorithm for assigning dynamic high-priority delivery tasks to the UAVs of the network. During the bidding phase of each UAV's regular delivery task allocation process, the UAV acts as an auctioneer for the dynamic task that is being broadcasted.

Algorithm 3 presents the auction-based algorithm for assigning re-charge tasks to the UAVs of the network whose energy stored in the battery is smaller than the required minimum energy level, E_{MIN}, plus a threshold factor.

3.2. Risk-Aware Path Planning

The flyable UAV paths connecting the UAV locations to the task locations are generated by means of a sampling-based path planning algorithm that samples a risk map of the operational area. The approach is taken from previous works since the aerial risk-aware path planning problem in urban environments has already been tackled. The problem of minimum-risk aerial path computation is decomposed in two steps. The first step consists of generating a 2D location-based risk map, which accounts for both the population density in the operational area and the UAV parameters (UAV mass, payload mass, UAV dimensions, UAV maximum speed, etc.). In the second step, a sampling-based algorithm based on the well-known RRT* algorithm computes the minimum-risk path in the map, minimizing both the overall risk associated with the computed path and the UAV flight time for that path. The risk map associates a risk value, expressed in expected fatalities per hour (h^{-1}), with each location. Since the planning algorithm returns, in general, sub-optimal risk-optimized paths, the average risk of each computed path is compared to an equivalent level of safety (ELOS) of 10^6 h^{-1}, as defined in [31]. After verifying the risk compatibility with respect to the ELOS, the computed path length is used in the energy computation function as a constant parameter. Further details about the risk map generation and the risk-aware path planning algorithm can be found in [32,33]. The risk-aware path planner is implemented in C++ using the ROS (Robot Operating System) framework.

Algorithm 1: Multi-Auctioneer Task Allocation Algorithm

for $i: 1 \longrightarrow N$ **do**
  UAV^i computes E_{MIN}^i
  UAV^i initializes $N_{DT_i}^A = 0, DS^i = 0, E_U^i = E_{MAX}^i$
end
$r = 1, again = 0$
while $r \leq M$ **do**
  UAV^N initializes $SoB^{d_t^r} = \oslash$
  for $i: 1 \longrightarrow N$ **do**
    $P_1^{d_t^r}(p, d_t^r, UAV^N \longrightarrow UAV^i)$
    UAV^i runs $Dynamic\_Tasks\_Auction$
    if $m^i \geq m_p^{d_t^r}$ **&** $T_i^i \leq T_{MAX}^{d_t^r}$ **do**
      UAV^i computes $L_1^{i,d_t^r}, L_2^{i,d_t^r}, \boldsymbol{V_{DT}^*}^{i,d_t^r}, E_{DT}^*\left(\boldsymbol{V_{DT}^*}^{i,d_t^r}\right)$
      $P_2^{d_t^r}(p, E_{DT}^*\left(\boldsymbol{V_{DT}^*}^{i,d_t^r}\right), UAV^i \longrightarrow UAV^N)$
      UAV^N updates $SoB^{d_t^r}$
    end
  end
  for $i: 1 \longrightarrow N$ **do**
    if $E_{DT}^*\left(\boldsymbol{V_{DT}^*}^{i,d_t^r}\right) = \min\left(SoB^{d_t^r}\right)$ **&** $N_{DT_i}^A - 1 \leq \vartheta(N_{DT}^A)_{j=1,\ldots,N\ (j\neq i)}$ **do**
      $P_3^{d_t^r}(p, d_t^r, UAV^N \longrightarrow UAV^i)$
      $P_4^{d_t^r}(p, d_t^r, UAV^i \longrightarrow UAV^N)$
      if $P_1^{d_t^r} = P_2^{d_t^r} = P_3^{d_t^r} = P_4^{d_t^r} = 1$ **do**
        d_t^r is assigned to UAV^i
        UAV^i updates $E_U^i = E_U^i - E_{DT}^*\left(\boldsymbol{V_{DT}^*}^{i,d_t^r}\right), T_i^i, U_L^i, N_{DT_i}^A$
      else
        UAV^N removes $E_{DT}^*\left(\boldsymbol{V_{DT}^*}^{i,d_t^r}\right)$ from $SoB^{d_t^r}$
        again = again + 1
      end
    end
  end
  for $i: 1 \longrightarrow N$ **do**
    UAV^i runs $Charge\_Tasks\_Auction$
  end
  if d_t^r has not been assigned **&** $again < 3N$ **do**
  else
    $again = 0$
    $r = r + 1$
  end
end

Algorithm 2: *Dynamic_Tasks_Auction* Algorithm

if dd_t^r is being broadcasted to UAV^i **&** dd_t^r has not been assigned **do**
  UAV^i initializes $SoB^{dd_t^r} = \oslash$
  for $g: 1 \longrightarrow N$ **do**
    $P_1^{dd_t^r}(p, dd_t^r, UAV^i \longrightarrow UAV^g)$
    if $m^g \geq m_p^{dd_t^r}$ **&** $T_i^g \leq T_{MAX}^{dd_t^r}$ **do**
      UAV^g computes $L_1^{g,dd_t^r}, L_2^{g,dd_t^r}, {V_{DT}^*}^{g,dd_t^r}, E_{DDT}^*\left({\boldsymbol{V_{DT}^*}}^{g,dd_t^r}\right)$
      $P_2^{d_t^r}(p, E_{DDT}^*\left({\boldsymbol{V_{DT}^*}}^{g,dd_t^r}\right), UAV^g \longrightarrow UAV^i)$
      UAV^i updates $SoB^{dd_t^r}$
    end
  end
  for $g: 1 \longrightarrow N$ **do**
    if $E_{DDT}^*\left({\boldsymbol{V_{DDT}^*}}^{g,dd_t^r}\right) = \min\left(SoB^{dd_t^r}\right)$ **do**
      $P_3^{dd_t^r}(p, dd_t^r, UAV^i \longrightarrow UAV^g)$
      $P_4^{dd_t^r}(p, dd_t^r, UAV^g \longrightarrow UAV^i)$
      if $P_1^{dd_t^r} = P_2^{dd_t^r} = P_3^{dd_t^r} = P_4^{dd_t^r} = 1$ **do**
        dd_t^r is assigned to UAV^g
        UAV^g updates $E_U^g = E_U^g - E_{DDT}^*\left({\boldsymbol{V_{DDT}^*}}^{g,dd_t^r}\right), T_i^g, U_L^g, N_{DT}^A{}_g$
      else
        UAV^i removes $E_{DDT}^*\left({\boldsymbol{V_{DDT}^*}}^{g,dd_t^r}\right)$ from $SoB^{dd_t^r}$
      end
    end
  end
end

Algorithm 3: *Charge_Tasks_Auction* Algorithm

if $E_U^i \leq +K_T E_{MAX}^i$ **do**
  UAV^i updates $DS = 1$
  $P_1^{c_t}(p, [U_L^i, DS^i = 1], UAV^i \longrightarrow UAV^N)$
  UAV^N initializes $SoB^{c_t} = \oslash$
  for $j: 1 \longrightarrow B$ **do**
    UAV^N computes bid $d^{j,i}$
    UAV^N adds $d^{j,i}$ to SoB^{c_t}
  end
  $P_2^{c_t}(p, SoB^{c_t}, UAV^N \longrightarrow UAV^i)$
  UAV^i computes $d^o = \min_{o=1,\ldots,B}(SoB^{c_t}), {\boldsymbol{V_{CT}^*}}^{i,c_t^o}$
  $P_4^{c_t}(p, DS^i = 0, UAV^i \longrightarrow UAV^N)$
  if $P_1^{c_t} = P_2^{c_t} = P_4^{c_t} = 1$ **do**
    c_t^o is assigned to UAV^i
    UAV^i updates $E_U^i = E_{MAX}^i, T_i^i, U_L^i, DS = 0$
  end
end

The proposed risk-aware path planning approach implements a high-fidelity risk assessment [32] considering the UAS parameters. Thus, the risk map changes according to the drone mass and the payload mass. Every time a UAV bids for a delivery task, two different risk maps are generated. The planning algorithm samples the first risk map to compute the risk-optimized path L_1, which corresponds to the first step of the delivery

process (the UAV moves from its start location to the pick-up location with no payload). Secondly, for the computation of L_2, the planning algorithm samples another risk map that accounts for the updated total mass of the UAV ($m + m_P$) in the risk computation. For this reason, it is necessary to evaluate a delivery task also considering the payload transported. The effect of the payload on the risk map and the resulting path can be observed in Figures 4 and 5. Figure 4 shows the risk map with a minimum-risk path considering a UAV type C without any additional payload. A similar scenario is reported in Figure 5, considering the same operational area and start and goal positions, but with a payload of 2.5 kg. Comparing Figures 4 and 5, we observed that the payload caused a higher risk in the risk map and, consequently, the resulting path changed. The involved risk is also shown in Figure 6, with the evolution of the risk along the paths with and without payload. Moreover, Figure 6 demonstrates the usefulness of the risk-aware path planning by comparing the minimum-risk path and the Line Of Sight (LOS) path. The LOS path is shorter but, on the contrary, provides a higher risk.

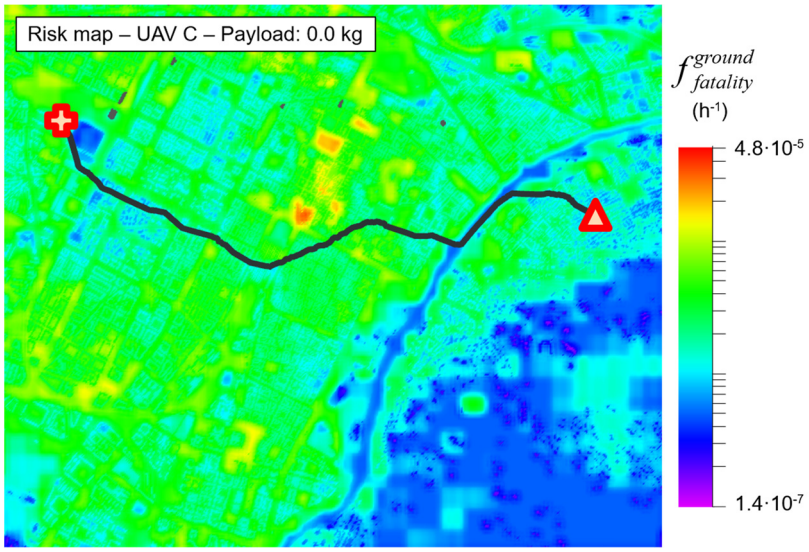

Figure 4. Risk map computed for a UAV type C without any additional payload. The black line is the minimum-risk path computed with the risk-aware path planning. The scenario refers to the simplified example of Figure 2.

The proposed approach is easily scalable to large urban areas. The risk map is generated by computing the risk for each cell (representing a location) in the map. Consequently, the computational complexity increases proportionally to the number of cells in the map and, therefore, with the dimension of the map. However, the resolution of the risk map can be adapted to manage large urban areas without excessively increasing the computational complexity.

The increase in the size of the risk map consequently also implies an increase in the computational complexity of the risk-aware path planning algorithm. The RRT*-based algorithm requires more nodes to both adequately explore the search space (i.e., the risk map) and obtain a near-optimal path. Therefore, as discussed in [34], the computational complexity of RRT* can be approximated to $O(n \log n)$, with n being the number of nodes sampled within the risk map.

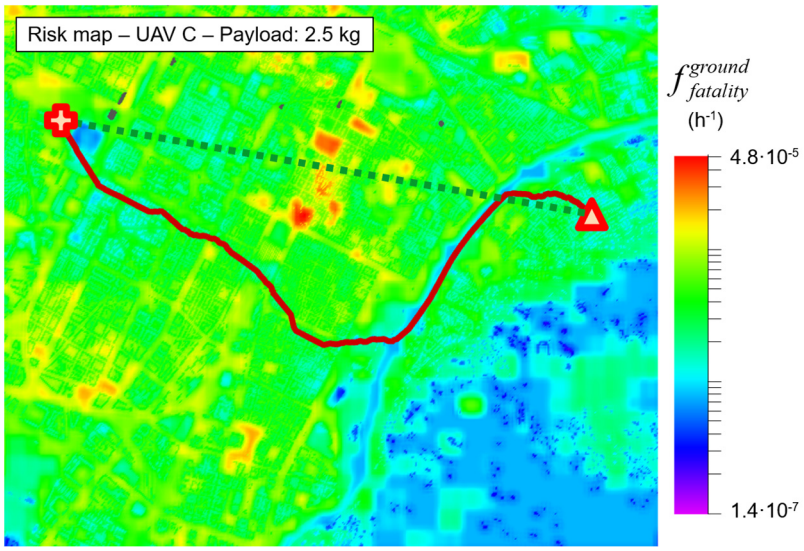

Figure 5. Risk map computed for a UAV type C carrying a payload of 2.5 kg. The red line is the minimum-risk path, while the dashed green line is the line-of-sight path. The scenario refers to the simplified example of Figure 2.

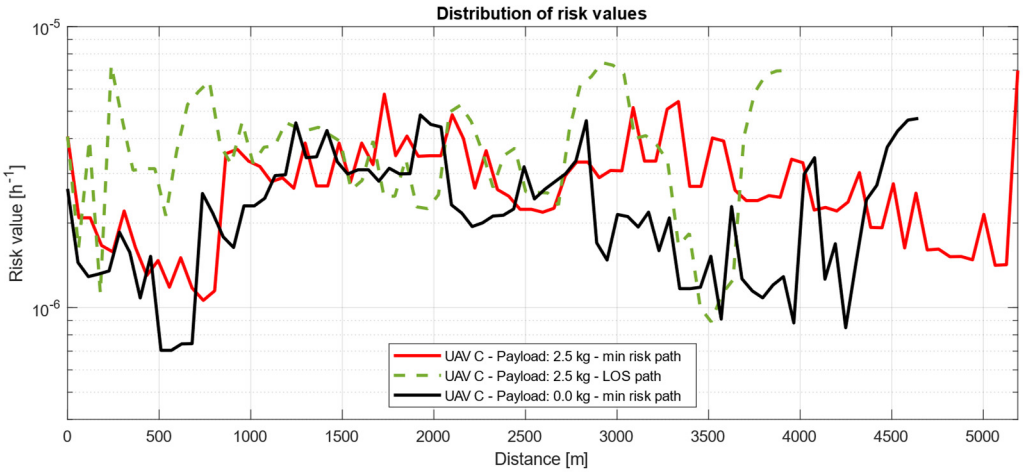

Figure 6. Distribution of risk values of the paths in Figures 4 and 5.

3.3. Energy Consumption Model

The energy consumption model is derived from the power consumption model proposed and validated in [35]. By merging such a power consumption model with the assumptions of Section 2, the resulting UAV energy consumption model can be defined as:

$$\begin{aligned} E_{DT}(\boldsymbol{V_{DT}}) = {} & E_i(mg, V_1, V_1, h) + E_p(mg, V_1, h) + E_i(mg, 0, V_2, L_1) + E_p(mg, V_2, L_1) + E_{par}(V_2, L_1) + E_i(mg, V_3, V_3, h) + \\ & E_p(mg, V_3, h) + E_i\big((m+m_p)g, V_4, V_4, h\big) + E_p\big((m+m_p)g, V_4, h\big) + E_i\big((m+m_p)g, 0, V_5, L_2\big) + E_p\big((m+ \\ & m_p)\,g, V_5, L_2\big) + E_{par}(V_5, L_2) + E_i\big((m+m_p)g, V_6, V_6, h\big) + E_p\big((m+m_p)g, V_6, h\big), \end{aligned} \tag{18}$$

for the completion of a delivery task, and as:

$$\begin{aligned} E_{CT}(m, \boldsymbol{V_{CT}}, d, h) = {} & E_i\big(mg, V_1', V_1', h\big) + E_p\big(mg, V_1', h\big) + E_i\big(mg, 0, V_2', d\big) + E_p\big(mg, V_2', d\big) + E_{par}(V_2', d) + \\ & E_i\big(mg, V_3', V_3', h\big) + E_p\big(mg, V_3', h\big), \end{aligned} \tag{19}$$

for the completion of a re-charge task. As far as dynamic tasks are concerned, $E_{DDT}(\boldsymbol{V_{DDT}}) = E_{DT}(\boldsymbol{V_{DDT}})$ since the conceptualization of the delivery phases does not change. In particular, $E_i(T, V_v, V, L) = T\left[\frac{V_v}{2} + \sqrt{\left(\frac{V_v}{2}\right)^2 + \frac{T}{2\rho A_r}}\right]\frac{L}{V}$ refers to the induced energy component (to propel air downward), $E_p(T, V, L) = \sqrt{b^3}c_d N_b c \rho \frac{R^4}{8}\sqrt{T^3}\frac{L}{V}$ refers to the profile energy component (to resist rotational drag due to the rotation of the propellers), and

$E_{par}(V, L) = \frac{1}{2} c_d \rho A_d V^2 L$ refers to the parasite energy component (to resist drag during the relative translational motion of the UAV with respect to the wind), with L denoting the general path length and V denoting the general drone velocity. The proposed energy consumption model overestimates the energy consumed by a UAV during task execution since T does not depend on V in forward flight. Furthermore, such an energy consumption model is valid independently from the type of multi-rotor UAV configuration (quadrotor, hexarotor, etc.).

3.4. Numerical Optimization

According to the problem formulation in Section 2, an optimization problem has to be solved by each bidding UAV in order to compute the optimal velocity of task execution while respecting the constraints of the delivery system. It follows the standard representation of the nonlinear constrained optimization problems defining the optimal energy-aware execution of tasks in Section 2: $\min f(\boldsymbol{x})$, subject to the constraints $\boldsymbol{g}(\boldsymbol{x}) \leq \mathbf{0}$, with $\boldsymbol{x} \in R^n$, $f(\boldsymbol{x}): R^n \longrightarrow R$, $\boldsymbol{g}(\boldsymbol{x}): R^n \longrightarrow R^m$. All the optimization problems stated in Section 2 can be brought in the standard form, with m being equal to the number of constraints of the problem stated for task for which the UAV is bidding during the allocation process, n being equal to the number of phases of the task, $\boldsymbol{x}$ being equal to either $\boldsymbol{V_{CT}}$ or $\boldsymbol{V_{DT/DDT}}$, and f being the objective function of the task. Both the UAVs' parameters and the tasks' parameters appear as constants in the optimization problems, except for the task execution velocity, which has to be optimized. Algorithm 4 shows the implementation of the constrained optimization algorithm based on a numerical Penalty Function (PF) Sequential Unconstrained Optimization (SUO) method.

Algorithm 4: PF-based SUO Algorithm

Result: $\boldsymbol{x}_*^k,\ flag$
Initialization: $\xi = 0.1,\ k = 0,\ \mu = 0.01,\ \boldsymbol{x}_*^{\mathbf{0}} = \mathbf{0},\ \boldsymbol{\rho^0} = \mathbf{1},\ \boldsymbol{\lambda^0} = \mathbf{0},$
$N_{ITER} = 100,\ q_1 = 2,\ q_2 = 0.5,\ q_3 = 5,\ flag = 0$
while $k < N_{ITER} \wedge flag = 0$ **do**
  $P(\boldsymbol{x}^k, \boldsymbol{\lambda}^k, \boldsymbol{\rho}^k) = \frac{f(\boldsymbol{x}^k)}{E_{MAX}} + \sum_{i=1}^{m} max\left(\frac{1}{2}\lambda_i^k + \rho_i^k g_i(\boldsymbol{x}^k), 0\right)^2$
  $k = k + 1$
  $\boldsymbol{x}_*^k = \arg\min P(\boldsymbol{x}_*^{k-1}, \boldsymbol{\lambda}^{k-1}, \boldsymbol{\rho}^{k-1})$
  for $i: 1 \longrightarrow m$ **do**
    $\lambda_i^k = \max\left(\lambda_i^{k-1} + q_1 \rho_i^{k-1} g_i(\boldsymbol{x}_*^k), 0\right)$
    if $|\lambda_i^k - \lambda_i^{k-1}| < q_2$ **do**
      $\rho_i^k = q_3 \rho_i^{k-1}$
    else
      $\rho_i^k = \rho_i^{k-1}$
    end
  end
  if $\|\boldsymbol{x}_*^k - \boldsymbol{x}_*^{k-1}\| < \mu$ **&** $\boldsymbol{g}(\boldsymbol{x}_*^k) \leq \mathbf{0}$ **&** $|f(\boldsymbol{x}_*^k) - f(\boldsymbol{x}_*^{k-1})| < \xi$ **do**
    $flag = 1$
  end
end

SUO algorithms iteratively perform unconstrained optimization on an enhanced objective function that includes the constraints of the original constrained optimization problem [36]. In this case, the enhanced objective function, $P(\boldsymbol{x}, \boldsymbol{\lambda}, \boldsymbol{\rho})$, is defined as the sum of the normalized objective function of the constrained problem, $\frac{f(\boldsymbol{x}^k)}{E_{MAX}}$, and the constraint-dependent penalty term, $\sum_{i=1}^{m} max\left(\frac{1}{2}\lambda_i + \rho_i g_i(\boldsymbol{x}), 0\right)^2$, as in [37]. At each step, k, of unconstrained optimization on P, the penalty parameters $\boldsymbol{\lambda} = [\lambda_1, \lambda_2, \ldots, \lambda_m]$ and

$\boldsymbol{\rho} = [\rho_1, \rho_2, \ldots, \rho_m]$ are updated depending on constraint-satisfaction-based criteria. A finite convergence to a sub-optimal solution can be achieved for finite penalty parameters, the latter of which should not be excessively increased in order to avoid numerical problems. The variation in the penalty parameters at each iteration depends on the parameters q_1, q_2, and q_3. The convergence speed of the algorithm depends on q_1, q_2, q_3, , and ξ. The termination condition of the proposed PF-based SUO algorithm depends on both the constraint satisfaction and tolerance parameters, and ξ. The average execution time of Algorithm 4 is 0.4 s. The unconstrained optimization performed on the PF exploits the *fminsearch(·)* MATLAB function. This optimizer implements the Nelder–Mead simplex algorithm, as defined in [38]. Considering that $P(\boldsymbol{x}, \boldsymbol{\lambda}, \boldsymbol{\rho})$ is at least a three-dimensional function, there is no theoretical guarantee that Algorithm 2 converges to the global optimum of the constrained problem. Figure 7 shows the evolution of both P and f throughout the bidding process of a UAV type A for the delivery task 2 in the simplified scenario of Figure 2.

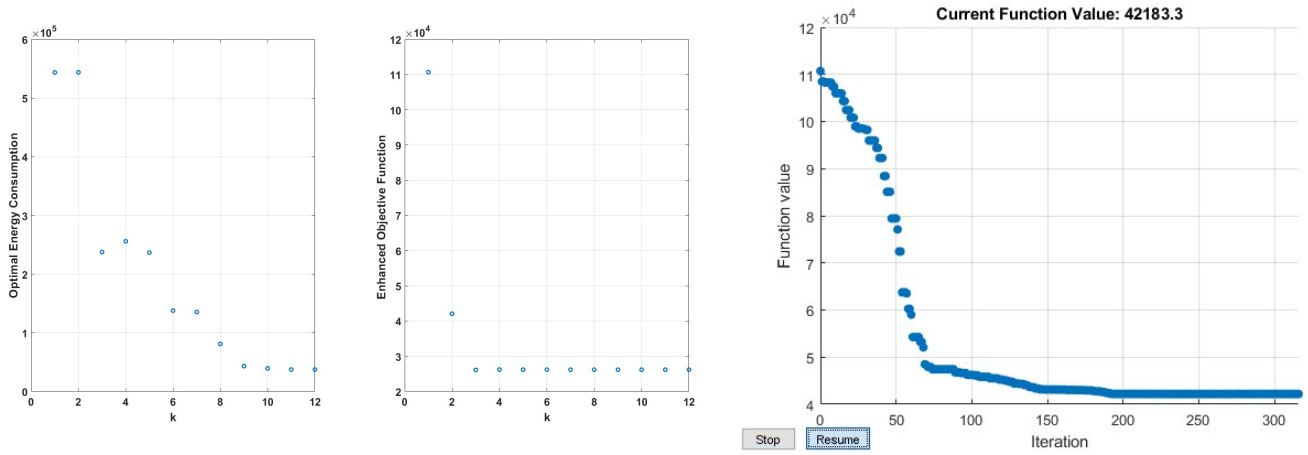

(**a**) (**b**)

Figure 7. (**a**) $E_{DT}(\boldsymbol{V_{DT}})$ optimization for the computation of the bid of UAV type A for delivery task 2. On the left, evolution of the constrained problem's objective function, $f(\boldsymbol{x})$, at each iteration, k, of Algorithm 4. On the right, evolution of the penalty function, $P(\boldsymbol{x}, \boldsymbol{\lambda}, \boldsymbol{\rho})$, at each iteration, k, of Algorithm 4. (**b**) Evolution of the penalty function, $P(\boldsymbol{x}, \boldsymbol{\lambda}, \boldsymbol{\rho})$, between $k = 1$ and $k = 2$ with respect to Figure 7a.

4. Simulation Results

In order to demonstrate the capability of the proposed market-based task allocation strategy to efficiently handle planning and allocation of delivery tasks, re-charge tasks, and dynamic tasks with different priorities and constraints, a whole set of simulation campaigns was designed for an operational area, defined as a squared populated portion of the city of Turin, Italy. As far as the operational area is concerned, the latitude and longitude extremities of the area where the aerial delivery fleet operates are $[45.0414°, 45.0769°]$ and $[7.6527°, 7.7134°]$ respectively. The height of flight h is limited to the range [50, 120] m. The aerial delivery fleet of UAVs is composed by $N = 5$ different UAVs, whose characteristics are reported in Table 1. The parameters reported in Table 1 were both taken from publicly available datasets and, when not available, linearly interpolated to fill in all the values.

Table 1. Parameters of the delivery fleet of UAVs.

UAV Type	A	B	C	D	E
m (kg)	1	2	3	4	5
A_r (m^2)	0.2	0.28	0.36	0.44	0.52
A_d (m^2)	0.4	0.6	0.8	1	1.2
c_d	0.1	0.2	0.3	0.4	0.5
b (kg·m)	0.001	0.002	0.003	0.004	0.005
c (m)	0.01	0.02	0.03	0.04	0.05
R (m)	0.1	0.12	0.15	0.18	0.21
V_{MAX} (m/s)	16	19	20	22	24
E_{MAX} (MJ)	0.68	0.9	1.17	1.43	1.67

The "regular" delivery tasks set was defined by a set of $M = 36$ tasks, with 6 tasks for each category of the 5 payload classes considered in the simulation campaigns: (0.5, 0.8, 1.0, 1.5, and 2.0 kg). The "dynamic" delivery tasks set was defined by a set of 6 tasks, with 1 task for each category of the 5 payload classes. Those tasks were advertised at random time instants between the start and the end of the main task allocation process. $B = 4$ charge hubs were assumed to be present within the operational area of reference. The time needed to fully re-charge a UAV with no residual energy in the battery was set to 0.5 h. Also, $K_T = 0.1$, $d_{MAX} = 6.2$ km, $\Delta T_{MAX} = 0.30$ h, and $\rho = 1.3$ kg·m^{-3}. The simulation campaigns designed to corroborate the validity of the approach were based on Monte Carlo simulations, repeated with four different scenarios:

- Scenario S_A: $T_{MIN} = 0$, and random initialization of the following parameters: initial U_L, delivery tasks' pick-up and delivery locations, h associated to each task, re-charge hubs' locations, and T_{MAX} (within the range of $[0,\ 3]$ h).
- Scenario S_A^*: analogous to S_A, but with no resource sharing in the allocation strategy and with each phase of task execution being completed at maximum speed.
- Scenario S_B: random initialization of the following parameters: initial U_L, delivery tasks' pick-up and delivery locations, h associated to each task, re-charge hubs' locations, T_{MAX} (within the range of $[0,\ 3]$ h), and T_{MIN} (within the range of $[1,\ 3]$ h).
- Scenario S_B^*: analogous to S_B, but with no resource sharing in the allocation strategy and with each phase of task execution being completed at maximum speed.

Tasks are advertised by the auctioneer according to ascending values of T_{MAX} so that tasks with higher priority in terms of due date are executed earlier. The results in terms of mean value (ϑ) and standard deviation (δ) of a set of well-defined output schedule parameters (N_{DT}^U, N_{DDT}^U, N_{CT}, and N_{DTi}^A) are derived from 50 simulations repeated for each scenario. In this case, the communication among the UAVs is assumed to be ideal ($p = 0$). Such results are reported in Table 2.

Table 2. Simulation results with ideal communication.

Scenario	E_{TOT} [MJ]		N_{DT}^U		N_{DDT}^U		N_{CT}		$\vartheta(N_{DT}^A)_i$					$\delta(N_{DT}^A)_i$				
	ϑ	δ	ϑ	δ	ϑ	δ	ϑ	δ	A	B	C	D	E	A	B	C	D	E
S_A	7.21	1.29	3	1.7	0	0	3	1	7	6	6	5	5	0.2	0.3	0.2	0.1	0.1
S_A^*	37.86	1.36	1	1.24	0	0	20	1.18	9	8	7	4	3	0.6	0.7	0.6	0.8	0.4
S_B	6.96	1.11	5	1.89	0	0	2	1.3	6	7	6	5	5	0.3	0.4	0.2	0.1	0.1
S_B^*	34.59	1.98	1	1.36	0	0	21	2.4	9	9	7	4	3	0.5	0.8	0.7	0.5	0.6

The impact of communication failures on the output schedule parameters was also investigated. Sets of 50 Monte-Carlo-based simulation campaigns were performed up to a 50% probability of communication failure by considering 1 particular instance for each of the 2 scenarios of reference (S_A and S_B). The simulation results are reported in Tables 3 and 4.

Table 3. Simulation results with lossy communication for an instance of scenario S_A.

p	E_{TOT} [MJ]		N^U_{DT}		N^U_{DDT}		N_{CT}		$\vartheta(N^A_{DT})_i$					$\delta(N^A_{DT})_i$				
	ϑ	δ	ϑ	δ	ϑ	δ	ϑ	δ	**A**	**B**	**C**	**D**	**E**	**A**	**B**	**C**	**D**	**E**
0	6.74	0	3	0	0	0	3	0	7	6	7	6	6	0	0	0	0	0
0.1	6.71	0.58	3	0	0	0	3	0	7	6	7	6	6	0.1	0.1	0.2	0.1	0.1
0.2	6.52	0.43	4	0.67	0	0	3	0	6	6	7	6	6	0.2	0.2	0.1	0.2	0.2
0.3	6.49	0.67	4	0.54	1	0.17	3	0.32	7	4	6	5	5	0.3	0.3	0.3	0.3	0.4
0.4	6.15	0.72	5	0.74	1	0.51	2	0.39	6	4	5	3	5	0.4	0.5	0.4	0.4	0.4
0.5	5.95	0.64	6	1.20	2	0.84	2	0.54	5	4	5	3	5	0.5	0.6	0.5	0.3	0.4

Table 4. Simulation results with lossy communication for an instance of scenario S_B.

p	E_{TOT} [MJ]		N^U_{DT}		N^U_{DDT}		N_{CT}		$\vartheta(N^A_{DT})_i$					$\delta(N^A_{DT})_i$				
	ϑ	δ	ϑ	δ	ϑ	δ	ϑ	δ	**1**	**2**	**3**	**4**	**5**	**1**	**2**	**3**	**4**	**5**
0	6.33	0	6	0	0	0	2	0	6	7	6	5	5	0	0	0	0	0
0.1	6.33	0.32	6	0	0	0	2	0	6	7	6	5	5	0.2	0.1	0.1	0.1	0.1
0.2	6.21	0.38	6	0.34	0	0	2	0	6	7	6	4	5	0.2	0.2	0.2	0.1	0.1
0.3	5.87	0.55	8	0.68	1	0.24	2	0.43	5	6	5	4	5	0.3	0.4	0.4	0.3	0.3
0.4	5.55	0.77	9	0.93	1	0.34	1	0.78	5	4	4	3	5	0.4	0.5	0.6	0.5	0.4
0.5	4.78	0.81	10	1.54	2	0.75	1	0.48	4	3	4	2	5	0.6	0.6	0.6	0.3	0.4

As far as the results with ideal communication are concerned, the capability of the proposed approach to handle a demanding task set was corroborated by the Monte-Carlo-based simulation campaign. The medium energy consumption decreased by 81% from the comparison of S_A and S^*_A, and by 80% from the comparison of S_B and S^*_B. The medium number of assigned re-charge tasks decreased by 85% from the comparison of S_A and S^*_A, and by 90.5% from the comparison of S_B and S^*_B. Scenarios S^*_A and S^*_B were conceived to show that, even with highly demanding task sets and the presence of dynamic tasks in the allocation loop, an energy-aware allocation of tasks was preferred over a simpler auction-based allocation with UAVs operating at maximum speed. The proposed market-based allocation architecture allowed the aerial fleet to evenly self-balance the distribution of the allocated delivery tasks, while minimizing the total energy consumption of the fleet and reducing the number of re-charge tasks to be executed by the fleet. This was reflected by mean and standard deviation values of N^A_{DT}, which increased in relative difference from $S_{A/B}$ to $S^*_{A/B}$. Obviously, with the task sets of both scenario S_A and scenario S_B being highly demanding ones, with tens of random parcel deliveries to be completed within close random time deadlines, a few more tasks remained unassigned when the results were compared to S^*_A and S^*_B. The higher variability in the distribution of tasks in the fleet in terms of ϑ and δ for scenarios S^*_A and S^*_B was due to the lack of the resource sharing condition $\left(N^A_{DTi} - 1 \leq \vartheta\left(N^A_{DT}\right)_{j=1,\ldots,\ N\ (j\neq i)}\right)$ in the bidding phase of each UAV.

As far as the results with lossy communication are concerned, the proposed allocation architecture featured superior robustness to fallible communication with respect to the one

proposed in our previous work in [30]. This was due to the redundancy of the allocation protocol when a task was not assigned due to message loss.

The results obtained with both the implementation of the aforementioned simulation campaigns and the analysis of the solution quality parameters (N_{DT}^{U}, N_{DDT}^{U}, N_{CT}, and N_{DTi}^{A}) enabled the following conclusions:

- The proposed architecture successfully tackled the formulated DDP with real-world instances of the problem itself.
- The main allocation objective of minimizing the energy consumption, despite being less favorable for the maximization of the number of completed tasks, did not compromise the level of performance of the allocation output.
- The proposed architecture was highly modular, flexible, and easily adaptable to tackle other task assignment problems with different objectives in the context of drone-based ITSs.
- Even with more demanding problem instances, such as scenario S_B^*, the allocation architecture's features of energy optimization, resource sharing, and dynamic task assignment did not compromise the overall level of performance of the architecture itself.
- The redundancy added in the allocation strategy enhanced the performances in case of lossy communication scenarios.

5. Conclusions

This work focused on presenting the development of a comprehensive combined task allocation and path planning architecture for managing a UAV-based intelligent transportation system in an urban environment. By inserting a nested variable-auctioneer auction-based allocation in the sequential single-item multi-auctioneer architecture, we showed that it is possible to both balance the distribution of tasks in the fleet and assign dynamic tasks during each round of the main task allocation process. This is particularly useful when a task with high priority, such as the aerial delivery of a medical sample, needs to be inserted in the allocation loop dynamically. The proposed allocation system proved to be able to efficiently allocate heterogenous tasks with time deadline constraints to a heterogenous fleet of multi-rotor UAVs. The architecture featured good robustness with respect to lossy communication scenarios.

Future works will be focused on validating the proposed approach by implementing the proposed protocol in a real fleet of UAVs. Also, future research directions can include a variety of simulation campaigns with other types of tasks and diverse urban environments, as well as a more in-depth analysis of the dynamic aspects of task allocation, including both final user-dependent tasks and real-time environment-dependent data.

Author Contributions: All authors contributed extensively to the current study. All authors have read and agreed to the published version of the manuscript.

Funding: This research received no external funding.

Data Availability Statement: The data used in the current study are available from the corresponding author upon reasonable request.

Acknowledgments: The authors wish to thank the Piedmont Aerospace Cluster (https://www.distrettoaerospazialepiemonte.com/en/) for supporting the Ph.D. activity of Marco Rinaldi.

Conflicts of Interest: The authors declare no conflicts of interest.

Nomenclature

m	UAV mass
m_P	Payload mass
V_v	UAV vertical velocity
T	Total thrust
ρ	Air density

A_r	Total propeller area
b	Thrust coefficient
c_d	Drag coefficient
N_b	Number of propeller blades
c	Blade width
R	Blade radius
A_d	UAV cross-section
V_{MAX}	UAV maximum speed
T_{MIN}	Minimum delivery task due date
T_{MAX}	Maximum delivery task due date
M	Number of delivery tasks
N	Number of multi-rotor UAVs
B	Number of charge hubs
p	Probability of communication failure
T_i	Time instant at which the UAV is available for task execution
U_L	UAV location
E_U	UAV residual energy
K_T	Threshold energy level above E_{MIN}, such that the UAV has to re-charge
d_t	Delivery task
dd_t	Dynamic delivery task
r_t	Re-charge task
DS	Discharged status, denoting if UAV needs to be charged (DS = 1) or not ($DS = 0$)
L_1	Path length from U_L to parcel pick-up location
L_2	Path length from parcel pick-up location to parcel delivery location
d	Path length from U_L to charge hub location
SoB	Set of bids in the allocation process
h	Height of flight
V_i	UAV velocity for execution of delivery task phase i
V_i'	UAV velocity for execution of re-charge task phase i
V_i''	UAV velocity for execution of dynamic delivery task phase i
E_{DT}	UAV energy consumption for delivery task
E_{CT}	UAV energy consumption for reaching the re-charge hub
E_{DDT}	UAV energy consumption for dynamic delivery task
E_{MIN}	UAV minimum residual energy for worst-case scenario
E_{MAX}	UAV maximum energy stored in the battery
d_{MAX}	Maximum path length from U_L to charge hub location in worst-case scenario
ΔT_{MAX}	Maximum flight time from U_L to charge hub location in worst-case scenario
$P_i(p_1, p_2, k \longrightarrow j)$	Phase P_i of the task allocation process, with probability of communication failure p_1, message p_2, and directivity from k to j. $P_i = 1$ if communication is successful; otherwise, $P_i = 0$
E_{TOT}	Total energy consumption associated with the output schedule
N_{DT}^U	Number of unassigned delivery tasks in the output schedule
N_{DDT}^U	Number of unassigned dynamic delivery tasks in the output schedule
N_{CT}	Number of assigned charge tasks in the output schedule
N_{DTi}^A	Number of delivery tasks assigned to a UAV type i in the output schedule
ϑ	Mean value
δ	Standard deviation

References

1. Menouar, H.; Guvenc, I.; Akkaya, K.; Uluagac, A.S.; Kadri, A.; Tuncer, A. UAV-Enabled Intelligent Transportation Systems for the Smart City: Applications and Challenges. *IEEE Commun. Mag.* **2017**, *55*, 22–28. [CrossRef]
2. Watkins, S.; Burry, J.; Mohamed, A.; Marino, M.; Prudden, S.; Fisher, A.; Kloet, N.; Jakobi, T.; Clothier, R. Ten questions concerning the use of drones in urban environments. *Build. Environ.* **2020**, *167*, 106458. [CrossRef]
3. Guo, J.; Chen, L.; Li, L.; Na, X.; Vlacic, L.; Wang, F.Y. Advanced Air Mobility: An Innovation for Future Diversified Transportation and Society. *IEEE Trans. Intell. Veh.* **2024**, *9*, 3106–3110. [CrossRef]
4. Straubinger, A.; de Groot, H.L.; Verhoef, E.T. E-commerce, delivery drones and their impact on cities. *Transp. Res. Part A Policy Pract.* **2023**, *178*, 103841. [CrossRef]

5. Pons-Prats, J.; Živojinović, T.; Kuljanin, J. On the understanding of the current status of urban air mobility development and its future prospects: Commuting in a flying vehicle as a new paradigm. *Transp. Res. Part E Logist. Transp. Rev.* **2022**, *166*, 102868. [CrossRef]
6. He, Y.; Wang, D.; Huang, F.; Zhang, R.; Min, L. Aerial-Ground Integrated Vehicular Networks: A UAV-Vehicle Collaboration Perspective. *IEEE Trans. Intell. Transp. Syst.* **2024**, *25*, 5154–5169. [CrossRef]
7. Hu, Z.; Chen, H.; Lyons, E.J.; Solak, S.; Zink, M. Towards sustainable UAV operations: Balancing economic optimization with environmental and social considerations in path planning. *Transp. Res. Part E Logist. Transp. Rev.* **2024**, *181*, 103314. [CrossRef]
8. Zarbakhshnia, N.; Ma, Z. Critical Success Factors for the Adoption of AVs in Sustainable Urban Transportation. *Transp. Policy* **2024**, *156*, 62–76. [CrossRef]
9. Telikani, A.; Sarkar, A.; Du, B.; Shen, J. Machine Learning for UAV-Aided ITS: A Review with Comparative Study. *IEEE Trans. Intell. Transp. Syst.* **2024**, 1–19. [CrossRef]
10. Rinaldi, M.; Primatesta, S.; Guglieri, G.; Rizzo, A. Auction-based Task Allocation for Safe and Energy Efficient UAS Parcel Transportation. *Transp. Res. Procedia* **2022**, *65*, 60–69. [CrossRef]
11. Tomasicchio, G.; Cedrone, A.; Fiorini, F.; Esposito, L.; Scardapane, G.; Filipponi, F.; Rinaldi, M.; Primatesta, S. Resilient Drone Mission Management and Route Optimization in Drone Delivery Context. In Proceedings of the 28th Ka and Broadband Communications Conference (Ka), Bradford, UK, 23–26 October 2023.
12. Rinaldi, M.; Primatesta, S.; Bugaj, M.; Rostáš, J.; Guglieri, G. Development of Heuristic Approaches for Last-Mile Delivery TSP with a Truck and Multiple Drones. *Drones* **2023**, *7*, 407. [CrossRef]
13. Poudel, S.; Moh, S. Task assignment algorithms for unmanned aerial vehicle networks: A comprehensive survey. *Veh. Commun.* **2022**, *35*, 100469. [CrossRef]
14. Jia, X.; Meng, M.Q.-H. A survey and analysis of task allocation algorithms in multi-robot systems. In Proceedings of the 2013 International Conference on Robotics and Biomimetics (ROBIO), Shenzhen, China, 12–14 December 2013.
15. Skaltsis, G.M.; Shin, H.S.; Tsourdos, A. A survey of task allocation techniques in MAS. In Proceedings of the 2021 International Conference on Unmanned Aircraft Systems (ICUAS), Athens, Greece, 15–18 June 2021.
16. Khamis, A.; Hussein, A.; Elmogy, A. Multi-robot task allocation: A review of the state-of-the-art. *Stud. Comput. Intell.* **2015**, *604*, 31–51.
17. Nishira, M.; Ito, S.; Nishikawa, H.; Kong, X.; Tomiyama, H. An Integer Programming Based Approach to Delivery Drone Routing under Load-Dependent Flight Speed. *Drones* **2023**, *7*, 320. [CrossRef]
18. Huang, H.; Hu, C.; Zhu, J.; Wu, M.; Malekian, R. Stochastic Task Scheduling in UAV-Based Intelligent On-Demand Meal Delivery System. *IEEE Trans. Intell. Transp. Syst.* **2022**, *23*, 13040–13054. [CrossRef]
19. Cheng, Q.; Yin, D.; Yang, J.; Shen, L. An Auction-Based Multiple Constraints Task Allocation Algorithm for Multi-UAV System. In Proceedings of the 2016 International Conference on Cybernetics, Robotics and Control (CRC), Hong Kong, China, 19–21 August 2016.
20. Qiu, Y.; Jiang, H.; Li, Q.; Dong, X.; Ren, Z. Application of an Adapted Genetic Algorithm on Task Allocation Problem of Multiple UAVs. In Proceedings of the 2018 CSAA Guidance, Navigation and Control Conference (CGNCC), Xiamen, China, 10–12 August 2018.
21. Hu, X.; Wong, K.K.; Yang, K.; Zheng, Z. Task and Bandwidth Allocation for UAV-Assisted Mobile Edge Computing with Trajectory Design. In Proceedings of the 2019 Global Communications Conference (GLOBECOM), Waikoloa, HI, USA, 9–13 December 2019.
22. Otte, M.; Kuhlman, M.J.; Sofge, D. Auctions for multi-robot task allocation in communication limited environments. *Auton. Robot.* **2020**, *44*, 547–584. [CrossRef]
23. Cao, L.; Tan, H.S.; Peng, H.; Pan, M.C. Multiple UAVs hierarchical dynamic task allocation based on PSO-FSA and decentralized auction. In Proceedings of the 2014 IEEE International Conference on Robotics and Biomimetics (ROBIO), Bali, Indonesia, 5–10 December 2014.
24. Sujit, P.B.; Beard, R. Distributed Sequential Auctions for Multiple UAV Task Allocation. In Proceedings of the 2007 American Control Conference, New York, NY, USA, 9–13 July 2007.
25. Li, X.; Liang, Y. An Optimal Online Distributed Auction Algorithm for Multi-UAV Task Allocation. In Proceedings of the 11th International Conference on Logistics, Informatics and Service Sciences (LISS), Jinan, China, 23–26 July 2021.
26. Sujit, P.B.; Beard, R. Multiple uav task allocation using distributed auctions. In Proceedings of the AIAA Guidance, Navigation and Control Conference and Exhibit, Hilton Head, CA, USA, 20–23 August 2007.
27. Xu, S.; Yu, L.; Deng, X.; Tang, L. Task Allocation for Multiple Unmanned Aerial Vehicles Based on Combinatorial Auctions. In Proceedings of the 2021 IEEE International Conference on Unmanned Systems (ICUS), Beijing, China, 15–17 October 2021.
28. Lee, C.W.; Wong, W.P. Last-mile drone delivery combinatorial double auction model using multi-objective evolutionary algorithms. *Soft Comput.* **2022**, *26*, 12355–12384. [CrossRef]
29. Kim, J. Learning-based Second Price Auction for Distributed Delivery Scheduling in Smart and Autonomous Urban Air Mobility. In Proceedings of the 2022 13th International Conference on Ubiquitous and Future Networks (ICUFN), Barcelona, Spain, 5–8 July 2022.
30. Rinaldi, M.; Primatesta, S.; Guglieri, G.; Rizzo, A. Multi-Auctioneer Market-based Task Scheduling for Persistent Drone Delivery. In Proceedings of the 2023 International Conference on Unmanned Aircraft Systems (ICUAS), Warsaw, PL, USA, 6–9 June 2023.

31. Dalamagkidis, K.; Valavanis, K.P.; Piegl, L.A. On unmanned aircraft systems issues, challenges and operational restrictions preventing integration into the National Airspace System. *Prog. Aerosp. Sci.* **2008**, *44*, 503–519. [CrossRef]
32. Primatesta, S.; Rizzo, A.; la Cour-Harbo, A. Ground risk map for unmanned aircraft in urban environments. *J. Intell. Robot. Syst.* **2020**, *97*, 489–509. [CrossRef]
33. Primatesta, S.; Guglieri, G.; Rizzo, A. A risk-aware path planning strategy for UAVs in urban environments. *J. Intell. Robot. Syst.* **2019**, *95*, 629–643. [CrossRef]
34. Karaman, S.; Frazzoli, E. Sampling-based algorithms for optimal motion planning. *Int. J. Robot. Res.* **2011**, *30*, 846–894. [CrossRef]
35. Liu, Z.; Sengupta, R.; Kurzhanskiy, A. A power consumption model for multi-rotor small unmanned aircraft systems. In Proceedings of the 2017 International Conference on Unmanned Aircraft Systems (ICUAS), Miami, FL, USA, 13–16 June 2017.
36. Byrne, C. Sequential unconstrained minimization algorithms for constrained optimization. *Inverse Probl.* **2008**, *24*, 015013. [CrossRef]
37. Available online: https://www.researchgate.net/publication/255602767_Methods_for_Constrained_Optimization (accessed on 9 May 2024).
38. Lagarias, J.C.; Reeds, J.A.; Wright, M.H.; Wright, P.E. Convergence Properties of the Nelder-Mead Simplex Method in Low Dimensions. *SIAM J. Optim.* **1998**, *9*, 112–147. [CrossRef]